RSC Advances

This is an *Accepted Manuscript*, which has been through the Royal Society of Chemistry peer review process and has been accepted for publication.

Accepted Manuscripts are published online shortly after acceptance, before technical editing, formatting and proof reading. Using this free service, authors can make their results available to the community, in citable form, before we publish the edited article. This *Accepted Manuscript* will be replaced by the edited, formatted and paginated article as soon as this is available.

You can find more information about *Accepted Manuscripts* in the Information for Authors.

Please note that technical editing may introduce minor changes to the text and/or graphics, which may alter content. The journal's standard Terms & Conditions and the Ethical guidelines still apply. In no event shall the Royal Society of Chemistry be held responsible for any errors or omissions in this *Accepted Manuscript* or any consequences arising from the use of any information it contains.

ROYAL SOCIETY OF CHEMISTRY

www.rsc.org/advances

Influence of surface properties on the performance of $Cu(In,Ga)(Se,S)_2$ thin film solar cells using Kelvin probe force microscopy

JungYup Yang[a], Dongho Lee[a], KwangSoo Huh[a], SeungJae Jung[a], JiWon Lee[a], HeeChan Lee[a], DoHyun Baek[a], ByoungJune Kim[a], Dongseop Kim[a], Junggyu Nam,[*a] GeeYeong Kim[b] and William Jo[*b]

[a]*Photovoltaic Development Team, Samsung SDI, CheonanSi 331-300, Korea*

[b]*Department of Physics and New and Renewable Energy Research Center, Ewha Womans University, Seoul 120-750, Korea*

* Corresponding author's e-mail: zignamu@gmail.com

wmjo@ewha.ac.kr

Abstract

We have investigated the sulfurization process in the $Cu(In,Ga)(Se,S)_2$ (CIGSS) absorber layer fabricated by a two-step sputter and selenization/sulfurization method in order to make an ideal double-graded band-gap profile and increase the open circuit voltage (V_{oc}). The sulfurization process was controlled by temperature from 570 °C to 590 °C without changing H_2S gas concentration and reaction time. Although the energy band-gap of the CIGSS absorber layer was increased with increasing sulfurization temperature, the V_{oc} of the completed CIGSS device fabricated by 590 °C sulfurization

RSC Advances Accepted Manuscript

temperature has not increased. In order to investigate this abnormal V_{oc} behavior the CIGSS absorber layer was measured by local electrical characterization utilizing Kelvin probe force microscopy, especially in terms of grain boundary potential and surface work-function. Consequently, the abnormal V_{oc} behavior was attributes to the degradation of grain boundary passivation by the strong sulfurization process. The optimum sulfurization temperature plays an important role in enhancement of grain boundary passivation. It was also verified that the V_{oc} degradation in the CIGSS solar cell fabricated by two-step method is more influenced by the grain boundary passivation quality comparison with the slightly non-uniformity of material composition among grains.

RSC Advances Accepted Manuscript

Thin film chalcopyrite photovoltaic devices based on the compound Cu(In,Ga)Se_2 (CIGSe) recently have achieved power conversion efficiencies over 20 % in the laboratory.[1-3] Generally, the high performance CIGSe absorbers have an intentionally double graded band-gap profile via Ga grading for a multi-stage co-evaporation method and sulfur diffusion for a two-step sputter and selenization/sulfurization method in order to improve the charge collection probability and the junction quality, etc.[4-6] The co-evaporation methods are well-known processes with many reports in research field and present record efficiency of CIGSe solar cells.[2] However, there have been not many investigations about a two-step sputter and selenization/sulfurization method even though successfully commercialized Cu(In,Ga)$(Se,S)_2$ (CIGSS) module is produced by Solar Frontier K.K in Japan. One of the most critical factors on a two-step sputter and selenization/sulfurization process for the CIGSS absorber layer is a sulfurization step which is hard not only to control sulfur reaction because of very fast sulfur diffusion into an absorber layer at high temperature (generally above 500 °C), but also to have an influence on device performance in accordance with sulfurization level easily. If the CIGSS absorber layer was fabricated by a strong sulfurization process (such as high temperature, long time sulfurization, and high partial pressure of H_2S gas), the CIGSS absorber quality capable of achieving the high open-circuit voltage (V_{oc}) may be

RSC Advances Accepted Manuscript

obtained by the increase of S/(S+Se) (SSSe) and Ga/(Ga+In) (GGI) ratios. However, there have problems particularly occurring in the strong sulfurization process that the fill factor (FF) decreased because of the deterioration of P/N junction quality by sulfur surface etching effect.[7,8] Therefore, it is important to keep the absorber surface state in a good condition during a sulfurization step. However, there is a paucity of research reports with CIGSS surface state such as potential properties at a grain boundary, compositional uniformity, interface defect state, and grain boundaries passivation property, etc.

Kelvin probe force microscopy (KPFM) recently has been used to study electrical properties of photovoltaic devices which present surface states, such as work-function, potentials of grain boundary/intra-grain, and etc.[9-13] Furthermore, KPFM can directly measure the band bending on the grain boundary and also expect the electron-hole carrier transport near the grain boundaries in the absorber layer of the CIGSS thin-film solar cells.[14,15] The KPFM provides a non-destructive technique to measure the surface potential distribution in solar cell devices. The KPFM results in not only helping to optimize the charge separation and its contribution to the production photocurrents, but also providing a picture of the grain boundary potential profiles and surface state. The information is used to improve the efficiency of the solar cells.

RSC Advances Accepted Manuscript

In this paper, we have investigated a sulfurization process in the CIGSS absorber layer fabricated by two-step sputter and selenization/sulfurization method. The local surface states of the CIGSS layer were also investigated by KPFM especially on the potential distributions at grain boundaries and the surface work-function distribution in order to resolve the harmful effect of a strong sulfurization process. Finally, the correlations of sulfurization degree with grain boundary passivation are discussed.

Approximately 1.6 um thick CIGSS absorber was processed as follow, which consists of two fabrication processes. In the first fabrication process, $Cu_{0.72}Ga_{0.28}$ and In precursors were sequentially deposited by a DC sputter on the 300 nm thick Mo back electrode which was also deposited by a sputtering system on a cleaned high strain point glass at room temperature. The Cu/(Ga+In) composition was controlled by film thickness and were fixed at about 0.87. The second fabrication process forms the completed CIGSS structure by selenization and sulfurization is a chemical reaction process with H_2Se and H_2S gas, respectively. In this experiment, the sulfurization process was changed by temperature from 570 ˚C to 590 ˚C in order to control the diffusion of sulfur into the CIGSe absorber by sulfurization. The detail temperature profile of the selenization and sulfurization process is shown in Fig. 1. At the selenization stage, a graded band-gap CIGSe absorber was fabricated intentionally by

RSC Advances Accepted Manuscript

the selenization of metal precursors in H_2Se gas atmosphere, then as the sulfurization stage, a thin CIGSS surface layer was formed on the CIGSe absorber surface by sulfurization with a H_2S gas in order to prepare a double graded band-gap profile. Heterojunctions were formed by a chemical bath deposition (CBD) process of about 5 nm Zn(O,OH,S) buffer layer in order to reduce a shunt path and increase interface quality. The advantages of Zn based buffer layer are eco-friendly non-toxic material and improvement of absorption at short wavelength. One laser (P1) and two mechanical (P2 and P3) scribing techniques were applied to form a monolithic interconnection. The gap between P1 and P3 should be minimized to reduce the dead area at total module area. A transparent conducting oxide (TCO) top contact layer was deposited on the CBD buffer layer using low pressure chemical vapor deposition (LPCVD). Morphologies and microstructure of the absorber layer were measured by a field emission scanning emission microscopy (SEM). X-ray fluorescence (XRF) and glow discharge optical emission spectrometer (GD-OES) were used to detect the composition ratio and the depth profile in the CIGSS films, respectively. The solar cell performance were measured under AM 1.5, 100 mW/cm^2 illumination at 25 ℃. Optical response characteristic of solar cell was measured by external quantum efficiency (EQE) which was used to calculate energy band-gap (E_g). The bulk and surface crystal structure were

RSC Advances Accepted Manuscript

studied by X-ray diffraction (XRD) and grazing incidence X-ray diffraction (GIXRD), respectively. Local electrical properties of the CIGSS absorber layer were measured by KPFM, which utilize a commercial atomic force microscopy. A Pt/Ir coated tip was used for measuring the CIGSS layer. The surface potential and topography were decided under a non-contact mode. The detail KPFM measurements were described in detail elsewhere.[13,16] Results of comparison between the surface properties and the device performance, it is essential to understand the polycrystalline CIGSS solar cell characteristics.

The GD-OES depth profile of the CIGSS absorber layer shown in Fig. 2 present GGI, SSSe, and E_g profile. The CIGSS absorber layers were made with different sulfurization temperature from 570 °C to 590 °C when the other conditions were fixed. The GD-OES was applied on samples with removed window and buffer layers in order to evaluate the content and distribution of sulfur in the absorber layer. It is well-known that the E_g could be engineered by changing GGI and SSSe ratios in chalcopyrite compounds semiconductor.[17,18] For example, the E_g of the CIGSS absorber can be increased by substituting In and Se by Ga and S, respectively. It was verified by the GD-OES measurements that more sulfur elements were incorporated into the CIGSe absorber as the sulfurization was performed at higher temperature as shown in Fig. 2 (a). In addition,

RSC Advances Accepted Manuscript

Fig. 2 (b) shows that the Ga concentration at the absorber surface was increased by increasing sulfurization temperature. It was confirmed from GD-OES depth profile results that the E_g of CIGSS absorber was increased by increasing sulfurization temperature as shown in Fig. 2(c). The E_g profile was calculated using below equation.[20]

$$E_g = 0.98 + 0.167x^2 + 0.17y^2 + 0.023x^2y - 0.17xy^2 + 0.397xy + 0.31y + 0.523x$$

where x is the GGI ratio and y is the SSSe ratio. Figure 3 gives the E_g determination by differentiation of EQE curve[21] in order to obtain the E_g values more exactly. The raw data of external quantum efficiency is depicted in the inset of Fig. 3. The E_g of the CIGSS absorber was increased by increasing sulfurization temperature as similar to GD-OES results. The E_g of the CIGSS absorber layer fabricated with 570°C, 580 °C, and 590 °C sulfurization temperature are 1.15eV, 1.17eV, and 1.24eV, respectively.

Figure 4 shows the cross-sectional SEM images of the CIGSS solar cells fabricated with 570 °C, 580 °C, and 590 °C sulfurization temperatures. The CIGSS grain sizes are important for device performance, as smaller grain may lead to both unfavorable hopping based electron transport and stronger recombination at grain boundaries[22,23] as well as the grain size is related to Ga gradient profile.[23-25] In our samples, overall grain sizes of the CIGSS were slightly increased with increasing sulfurization temperature in

RSC Advances Accepted Manuscript

addition to a small grain area and void region adjacent to the Mo bottom electrode significantly decreased as the sulfurization temperature increased because higher Ga concentration generally tended to form smaller grain region.[26] This change in small grain area and void region of CIGSS films did not definitely affect power conversion efficiency, but these have effect on process window because of the correlation of adhesion strength between CIGSS and Mo layer.

The photovoltaic performances of the devices with three different sulfurization temperatures (570 °C, 580 °C, and 590 °C) were extracted from one sun current-voltage measurement. The results are shown in Fig. 5 and the characteristic device parameters are summarized in table I. Generally, the J_{sc} decrease with increasing the E_g and the V_{oc} increases as the E_g increases in photovoltaic devices. In our devices, the J_{sc} and V_{oc} depend on the absorber E_g apart from the V_{oc} of a device made by 590 °C sulfurization temperature as shown in Table I. In addition, in the highest sulfurization temperature, the lowest efficiency was observed due to the largely decrease of the FF. This result means that too much sulfur incorporation into the CIGSS absorber layer may lead to detrimental impacts on the FF because of deteriorated P/N heterojunction quality as mentioned above. Then, "Why the V_{oc} was decrease with 590 °C sulfurization temperature?" has been a major question in this experiment.

RSC Advances Accepted Manuscript

In order to analyze the abnormal behavior of the V_{oc}, the surface properties of the CIGSS absorber were investigated by KPFM, since the sulfurization temperature influences surface quality. Figure 6 (a) - (c) and (d) - (f) show the topography and surface potential images of the CIGSS absorber measured by KPFM, respectively. In Fig. 6 (d) - (f), the yellow and blue regions represent the positive potential value and negative potential, respectively. From the KPFM measurement, we can obtain surface work-function on the CIGSS absorber as follow. The KPFM measures contact potential difference (V_{CPD}) between a conducting atomic force microscope tip and the sample. We measured tip work function by using a highly ordered pyrolytic graphite. The V_{CPD} between the tip and sample is defined as; $V_{CPD} = (\phi_{tip} - \phi_{sample})/-e$ where ϕ_{sample} and ϕ_{tip} are the work-functions of the sample and tip, respectively, and e is the electronic charge. Figure 7 show the surface work-function distributions in the CIGSS absorber layer processed at different sulfurization temperature as calculated above function. The CIGSS work function value is around 4.5~5.5 eV. As shown in Fig. 7, the work-function distributions become narrow with increasing sulfurization temperature. This means that the surface state in the CIGSS absorber treated at higher sulfurization temperature is more uniform than that of the CIGSS absorber treated at lower sulfurization temperature. Many work-function peaks mean that diverse phases having

RSC Advances Accepted Manuscript

different compositional ratio might be existed at the surface.

In order to analyze about KPFM results more in detail, we have performed bulk and surface crystallization by XRD and GIXRD, respectively. Figure 8 presents the CuKα two-theta XRD patterns of the CIGSS absorber layer sulfurized at different temperatures. The overall range XRD spectra of the CIGSS absorber are shown in Fig. 8 (a). The preferred orientation for CIGSS samples were in (112) direction. The XRD intensity was higher than background at about 27° and a small peak can be seen at about 28°. This small peak indicates the existence of a separated Ga-rich CIGSS phase (dotted arrow in Fig. 8 (a) and (b)). The CIGSS absorber film sulfurized by high temperature showed the decrease of Ga-rich CIGSS peak intensity, indicating that the CIGSS absorber layer was improved depth compositional homogeneity and the formation of a high quality chalcopyrite phase. However, a shoulder peak occurs at the high angle side of the (112) and (220) reflection for the CIGSS sample, as indicated by solid-arrows in Fig. 8 (b) and (c) in addition to these shoulder peaks were decreased by increasing sulfurization temperature as shown in Fig. 8 (b) and (c). The shoulder peak is maybe caused by inhomogeneous sulfur composition between grains. Therefore, the increase of surfurization temperature makes more uniform sulfur composition between grains. The high sulfurization temperature also shows more uniform work function distribution as

RSC Advances Accepted Manuscript

previous shown in Fig. 7 (c). The uniform surface states such as narrow work function distribution are corresponding with uniform sulfur composition and better crystallinity of the CIGSS thin-films. Thus, the XRD results have something in common with as mentioned KPFM results.

Figure 9 presents GIXRD patterns of the CIGSS absorber on glass substrate fabricated by a basic surfurization process. Using the GIXRD mode the x-ray penetrates the absorber only close to the surface. Therefore, the GIXRD data provides information from the CIGSS near a surface layer, while the data from the conventional XRD data reveals little information from the film surface. The GIXRD scan was collected with a grazing incidence angle of 0.2°. The difference in overall range pattern between Fig. 8 (a) and Fig. 9 (a) is that intensity of the Mo peak (about 40°) was greatly reduced due to the almost reflecting surface properties by grazing incidence angle. Figure 9 (b) show enlarged a GIXRD pattern about (220) peak of the CIGSS. As shown in Fig. 9 (b), the shoulder peak was slightly decreased by increasing sulfurization temperature for the similar reason of as a mentioned normal XRD result. Therefore, the surface state in the CIGSS absorber with higher sulfurization temperature is also more uniform than CIGSS absorber sulfurized by low temperature.

RSC Advances Accepted Manuscript

Even though the CIGSS absorber layers were fabricated by high temperature sulfurization were become more and more uniform in composition between grains as presented KPFM, XRD, and GIXRD results, we still cannot solve the abnormal V_{oc} behavior for the CIGSS device processed by 590 °C surfurization. Therefore, we have investigated the potential distributions at grain boundary using KPFM in detail. Generally, the device performances in chalcopyrite thin film solar cells are closely connected to potential properties of a grain boundary.[27] Figure 10 shows the statistical potential distribution of the CIGSS absorber surface focusing on grain boundaries. Histograms of potential distribution are indicated at the grain boundaries based on KPFM data in the grain boundary of each samples. According to the previous result of the local electrical properties, the positive potential distributions at grain boundaries can be improved the device performance because the surface energy band at grain boundaries was bended by the positive potential at grain boundaries. The bended energy band plays an important role in passivation at grain boundaries.[13,26,28] From the results, we compared the number of the distribution rate of the potential of the each CIGSS thin film depending on the device performance, especially the V_{oc}. In Fig. 10, the CIGSS absorber layer fabricated by 580 °C sulfurization temperature shows 80% of positive surface potential ratio at grain boundaries, but the CIGSS processed by 590 °C

RSC Advances Accepted Manuscript

sulfurization temperature shows only 65%. The lowest positive potential barrier distributions reflects that the CIGSS sulfurized by 590 °C result in the recombination becomes increased at the grain boundaries, consequently, decrease V_{oc} compared with their energy band-gap. In order words, it was verified to be possible to more sulfur into the CIGSe absorber layer by adjusting the temperature of a sulfurization process but it is difficult to improve the device performance with high sulfur contained CIGSS absorber. Although the uniformity of materials composition among grains is better when the sulfurization temperature is increased and over the optimum point, the passivation characteristics at a grain boundary are degraded at over sulfurization. Hence, the V_{oc} loss is more significant due to the recombination at a grain boundary than composition uniformity. This also proposed that the existence of an upper limit of incorporated sulfur was a good indication to improve the passivation property at grain boundaries.

In conclusion, we have investigated the surface stats of the CIGSS absorber layer measured by the KPFM focusing on the potential distributions at a grin boundary and surface work-function distributions in order to optimize a sulfurization process in the CIGSS absorber layer fabricated by a two-step sputter and selenization/sulfurization method. The efficiency of 15.15 % is achieved on a 900 cm^2 sized module by 580 °C sulfurization temperature that is optimized condition in our experiment. The

RSC Advances Accepted Manuscript

sulfurization process at 580 °C temperature has improved a grain boundary passivation in surface of the CIGSS absorber, and result in a decreased V_{oc} loss. The experimental results also present that the V_{oc} loss by recombination at a grain boundary is more dominant comparison with the uniformity of materials composition among grains. In addition, there are upper limit of sulfur contents in CIGSS absorber layer due to the degradation of passivation quality at the grain boundary. Consequently, the passivation quality of surface grain boundaries may depend on the sulfurization process, and this plays a crucial role in the final device performance.

RSC Advances Accepted Manuscript

Acknowledgements

This work was supported by Korea Institute of Energy Technology Evaluation and Planning (KETEP) (grant no. 20119010100010) in 2011. This work was supported by the New & Renewable Energy of the Korea Institute of Energy Technology Evaluation and Planning (KETEP) grant funded by the Korea government, Ministry of Trade, Industry and Energy (No. 20123010010130).

RSC Advances Accepted Manuscript

References

1 Martin A. Green, Keith Emery, Yoshihiro Hishikawa, Wilhelm Warta, and Ewan D. Dunlop, *Prog. Photovolt: Res. Appl.*, 2015, **23**, 1.

2 P. Jackson, D. Hariskos, R. Wuerz, O. Kiowski, A. Bauer, T. M. Friedlmeier, and M. Powalla, *Physica Status Solidi (RRL)* , 2015, **9**, 28.

3 Chirila A, Reinhard P, Pianezzi F, Bloesch P, Uhl AR, Fella C, Kranz L, Keller D, Gretener C, Hagendorfer H, Jaeger D, Erni R, Nishiwaki S, Buecheler S, Tiwari AN, *Nature Materials,* 2013, **12**, 1107.

4 Yoshiaki Hirai1, Yasuyoshi Kurokawa, and Akira Yamada, *Jpn. J. Appl. Phys.*, 2013, **53**, 012301.

5 M. Troviano, K. Taretto, *25th European Photovoltaic Solar Energy Conference and Exhibition & 5th World Conference on Photovoltaic Energy Conversion*, 2010, 3318-3322.

6 Jiyon Song, Sheng S. Li, C.H. Huang, O.D. Crisalle, T.J. Anderson, *Solid-State Electronics*, 2004, **48**, 73.

RSC Advances Accepted Manuscript

7 Yuri Goushi *et al.*, *Sol. Energy Mater. Sol. Cells,* 2009, **93**, 1318.

8 Yoshinori Nagoya, Katsumi Kushiya, Muneyori Tachiyuki, Osamu Yamase, *Sol. Energy Mater. Sol. Cells*, 2001, **67**, 247.

9 T. Glatzel, D.F. Marron, T. Schedel-Niedrig, S. Sadewasser, M.C. Lux-Steiner, *Appl. Phys. Lett.*, 2002, **81**, 2017.

10 T. Glatzel, H. Steigert, S. Sadewasser, R. Klenk, M.C. Lux-Steiner, *Thin Solid Films*, 2005, **480**, 177.

11 S. Sadewasser, T. Glatzel, S. Schuler, S. Nishiwaki, R. Kaigawa, M.C. Lux-Steiner, *Thin Solid Films*, 2003, **431**, 257.

12 G. Hanna, T. Glatzel, S. Sadewasser, N. Ott, H.P. Strunk, U. Rau, J.H. Werner, *Appl. Phys. A*, 2006, **82**, 1.

13 G.Y. Kim *et al.*, *Sol. Energy Mater. Sol. Cells*, 2014, **127**, 129.

14 C.-S Jiang, R. Noufi, K. Ramanathan, J. A. AbuShama, H. R. Moutinho and M. M. Al-Jassim, *Appl. Phys. Lett.*, 2004, **85,** 2625.

15 A. R. Jeong, *Adv. Nat. Sci.: Nanosci. Nanotechnol.*, 2013, **4**, 015007.

RSC Advances Accepted Manuscript

16 W. Melitz, J. Shen, A. C. Kummel, S. Lee, *Surf. Sci. Rep.*,2011, **66**, 1.

17 *Cu($In_{1-x}Ga_x$)Se_2 based thin film solar cells*, Subba Ramaiah Kodigala, Elsevier: Academic Press, 2010.

18 *Thin film solar cells: next generation photovoltaics and its application*, Yoshihiri Hamakawa, , Springer, 2004.

19 M. Gloeckler, J. R. Sites, W. K. Metzger, *J. Appl. Phys.*, 2005, **98**, 113704.

20 Shu-Hao Chang, Ming-Yi Chiang, Chien-Chih Chiang, Fang-Wei Yuan, Chia-Yu Chen, Bo-Cheng Chiu, Tzu-Lun Kao, Chi-Huang Laic, and Hsing-Yu Tuan, *Energy & Environmental Science*, 2011, **4**, 4929.

21 *Handbook of Photovoltaic Science and Engineering, Chapter. Cu(InGa)Se_2 Solar Cells*, W. N. Shafarman and L. Stolt, , Wiley, 2003.

22 D. Azulay , O. Millo , I. Balberg , H. W. Schock , I. Visoly-Fisher, D. Cahen, *Sol. Energy Mater. Sol. Cells*, 2007, **91**, 85.

23 P.M.P.Salomé, A. Hultqvist, V. Fjällström, B. Vermang, M. Edoff, B. Aitken, K. Zhang, K. Fuller, C. Kosik Williams, *Sol. Energy Mater. Sol. Cells*, 2014, **123**, 166.

RSC Advances Accepted Manuscript

24 D. Abou-Ras, R. Caballero, C. A. Kaufmann, M. Nichterwitz, K. Sakurai1, S. Schorr, T. Unold and H. W. Schock, *Physica Status Solidi (RRL)*, 2008, **2**, 138.

25 S. Chaisitsak, A. Yamada, M. Konagai, *Jpn. J. Appl. Phys.*, 2002, **41**, 507.

26 J. B. Li, V. Chawla, B. M. Clemens, *Adv. Mater.*, 2012, **24**, 720.

27 C.-S Jiang, R. Noufi, K. Ramanathan, J. A. AbuShama, H. R. Moutinho and M. M. Al-Jassim, *Appl. Phys. Lett.*, 2004, **85**, 2625.

28 M. Hafemeister, S. Siebentritt, J. Albert, M. C. Lux-Steiner, S. Sadewasser, *Phys. Rev. Lett.*, 2010, **104**, 196602.

RSC Advances Accepted Manuscript

Table caption

Table I. CIGSS device characteristics were fabricated by different sulfurization process (570°C ~ 590°C). The listed are the device parameters: the efficiency (Eff.), open circuit voltage (V_{oc}), short circuit current (J_{sc}), series resistance (R_s), shunt resistance (R_{sh}), fill factor (FF), diode ideality factor (N-factor), and E_g.

RSC Advances Accepted Manuscript

Figure captions

Figure 1. The temperature profiles of two-step selenization/sulfurization process.

Figure 2. The (a) GGI and (b) SSSe GD-OES profile and (c) calculated E_g profile of CIGSS absorber layer fabricated by various sulfurization temperature.

Figure 3. d(QE)/dλ curve as a function of wavelength in order to determine the E_g. Inset figure is EQE raw data.

Figure 4. Cross-sectional SEM images of the CIGSS cells fabricated with different sulfurization temperature; (a) 570 °C, (b) 580 °C, and (c) 590 °C.

Figure 5. One-sun I-V curves of 900 cm^2 sized 64 series connected CIGSS device fabricated by different sulfurization temperatures. Black, red, and green lines are 570 °C, 580 °C, and 590°C sulfurization temperature, respectively.

Figure 6. (a) - (c) Topography images of the CIGSS absorber layer surface (d) - (f) surface potential mapping images of the corresponding topography.

Figure 7. Surface work-function distributions in CIGSS absorber layer processed at different sulfurization temperature; (a) 570 °C, (b) 580 °C, and (c) 590 °C.

RSC Advances Accepted Manuscript

Figure 8. Normal XRD spectra for CIGSS absorber layer on Mo-coated glass substrates with different sulfurization temperature. (a) The overall range of XRD pattern, enlarged view around (b) (112) peak, and (c) (220) peak of CIGSS absorber layer

Figure 9. GIXRD spectra in CIGSS sample prepared by the different sulfurization temperature showing (a) the overall range and (b) enlarged images around (220) peak of CIGSS absorber layer surface.

Figure 10. Statistical characterization of surface potential focusing on grain boundaries based on the line profiles results of in many regions of grain boundaries of CIGSS samples fabricated by different sulfurization temperature; (a) 570 °C, (b) 580 °C, and (c) 590 °C.

RSC Advances Accepted Manuscript

Table I. CIGSS device characteristics were fabricated by different sulfurization process (570°C ~ 590°C). The listed are the device parameters: the efficiency (Eff.), open circuit voltage (V_{oc}), short circuit current (J_{sc}), series resistance (R_s), shunt resistance (R_{sh}), fill factor (FF), and diode ideality factor (N-factor).

Temperature (℃)	Eff. (%)	V_{oc} (V)	J_{sc} (mA/cm^2)	FF (%)	R_s (Ωcm^2)	R_{sh} (Ωcm^2)	N-factor	Band-gap by QE (eV)
570	15.10	0.646	33.15	70.53	1.35	1363	1.51	1.15
580	15.15	0.669	31.63	71.62	1.26	1225	1.50	1.17
590	12.84	0.662	28.78	67.43	1.58	850	1.83	1.24

RSC Advances Accepted Manuscript

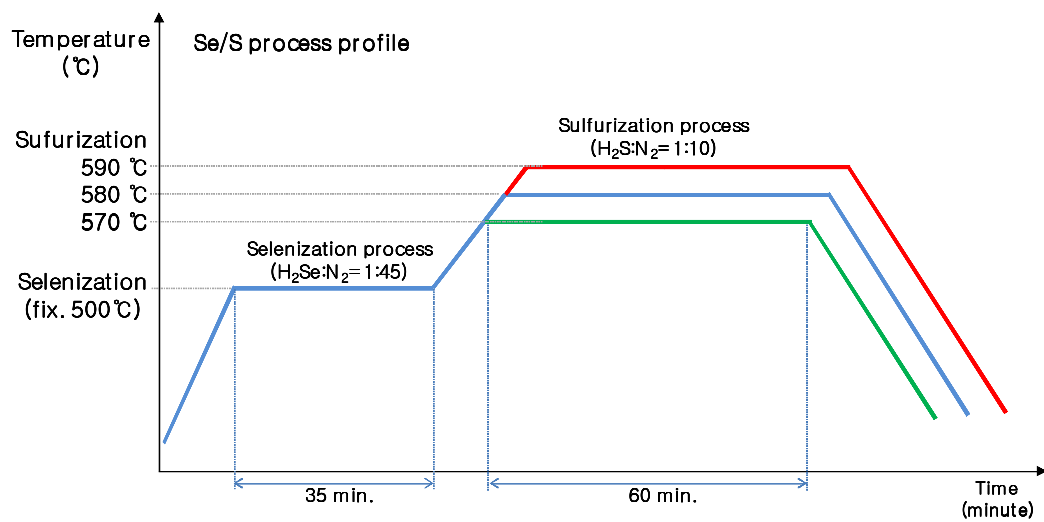

Figure 1. JungYup Yang *et al.*

RSC Advances Accepted Manuscript

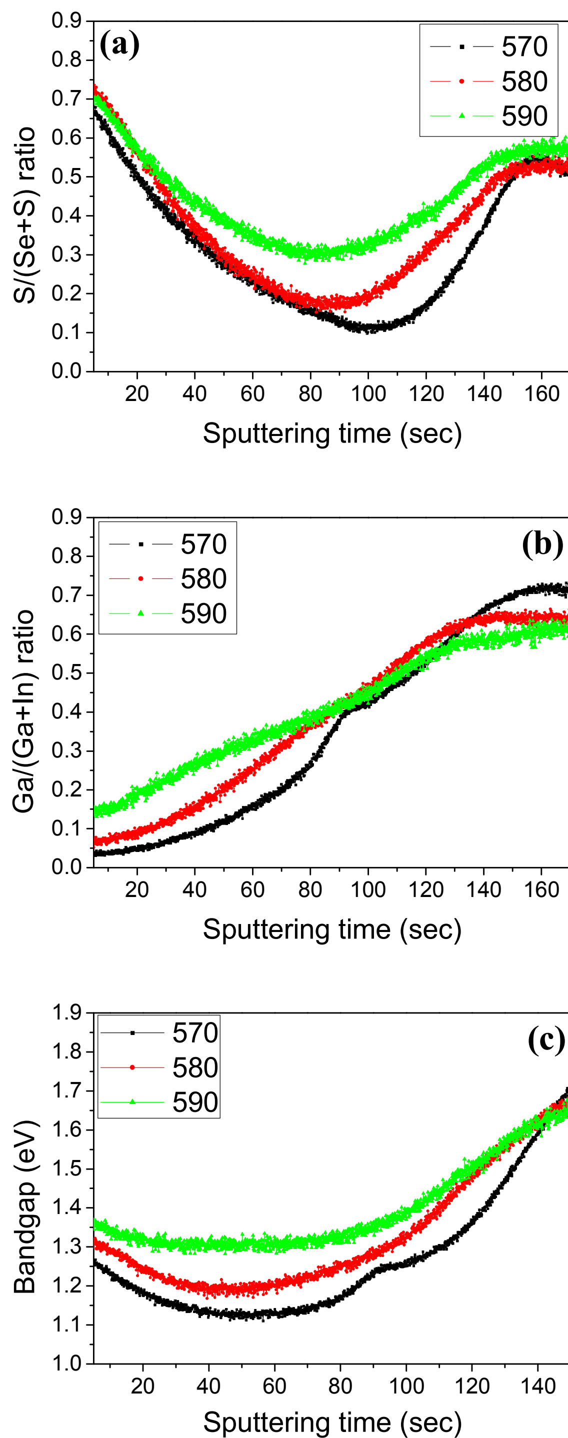

Figure 2. JungYup Yang *et al.*

RSC Advances Accepted Manuscript

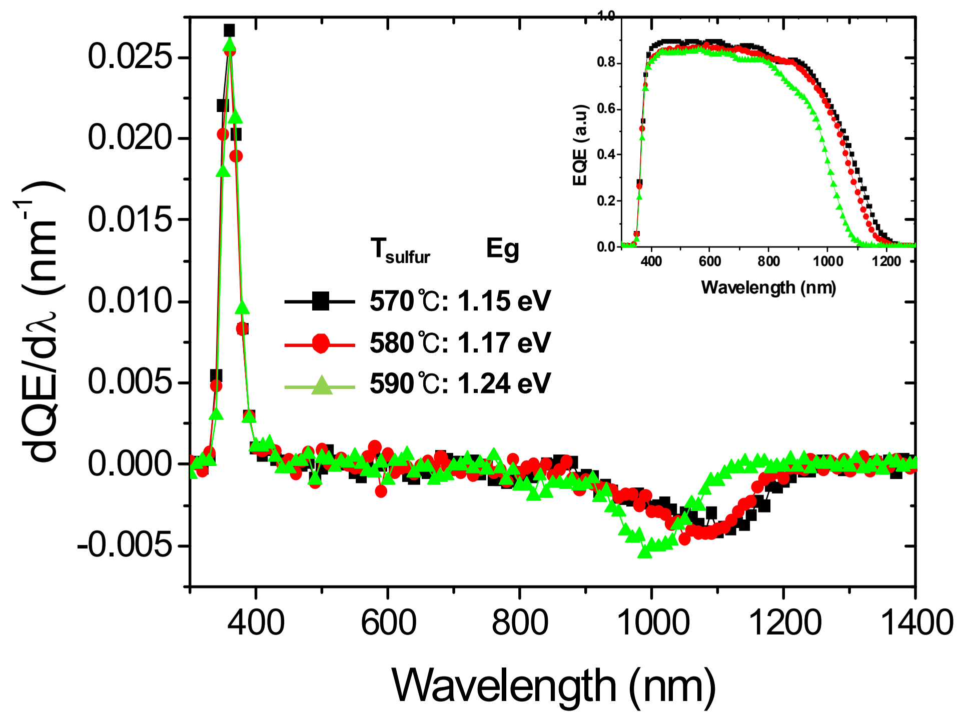

Figure 3. JungYup Yang *et al.*

RSC Advances Accepted Manuscript

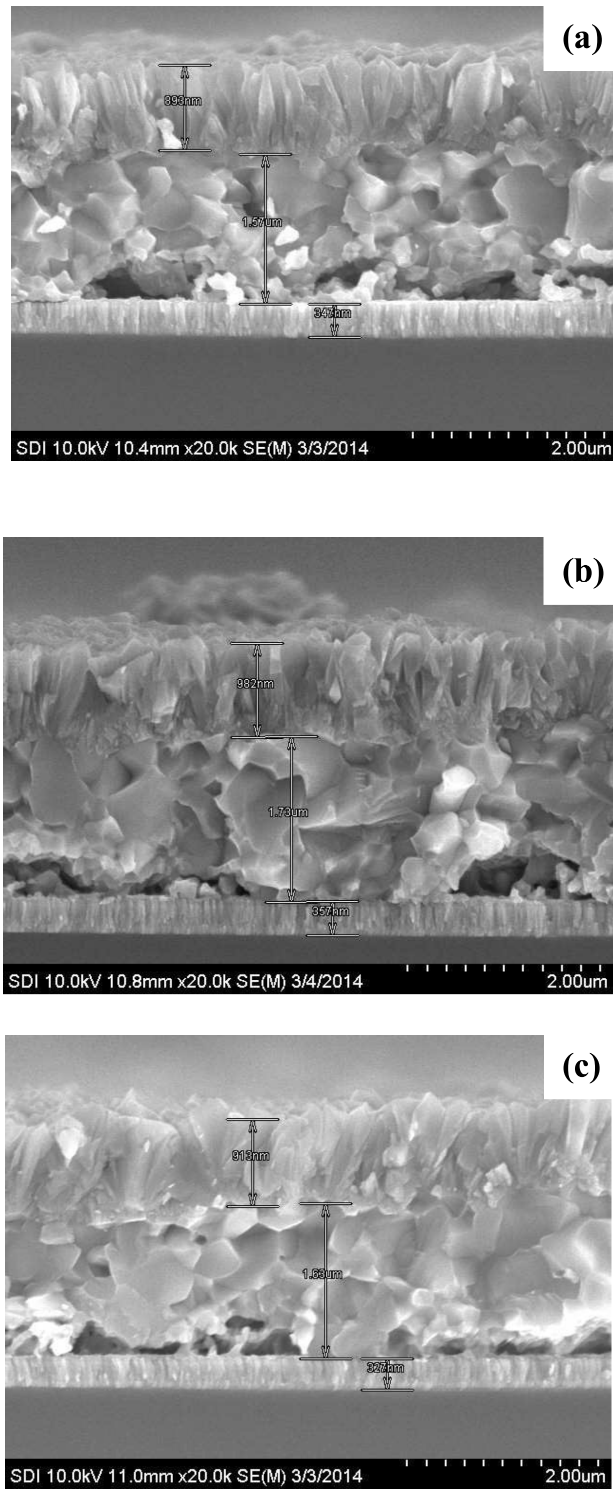

Figure 4. JungYup Yang *et al.*

RSC Advances Accepted Manuscript

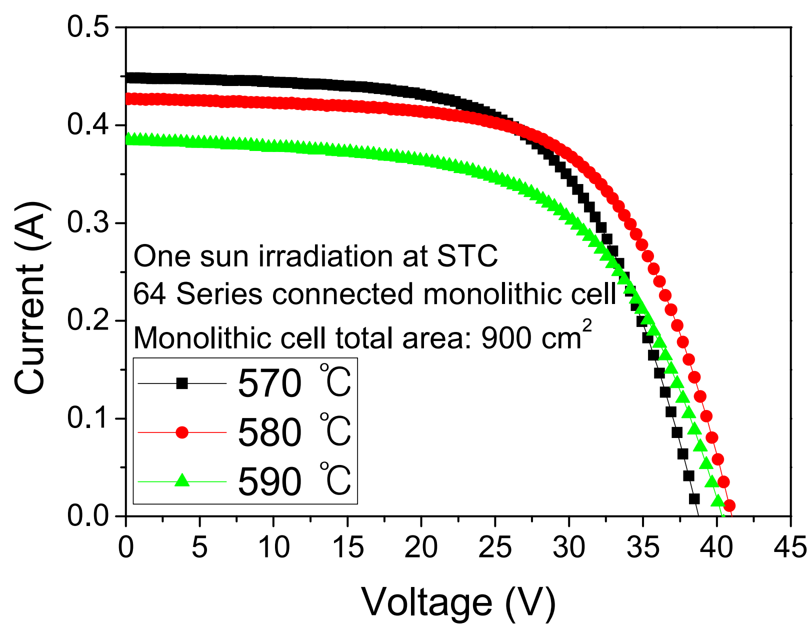

Figure 5. JungYup Yang *et al.*

RSC Advances Accepted Manuscript

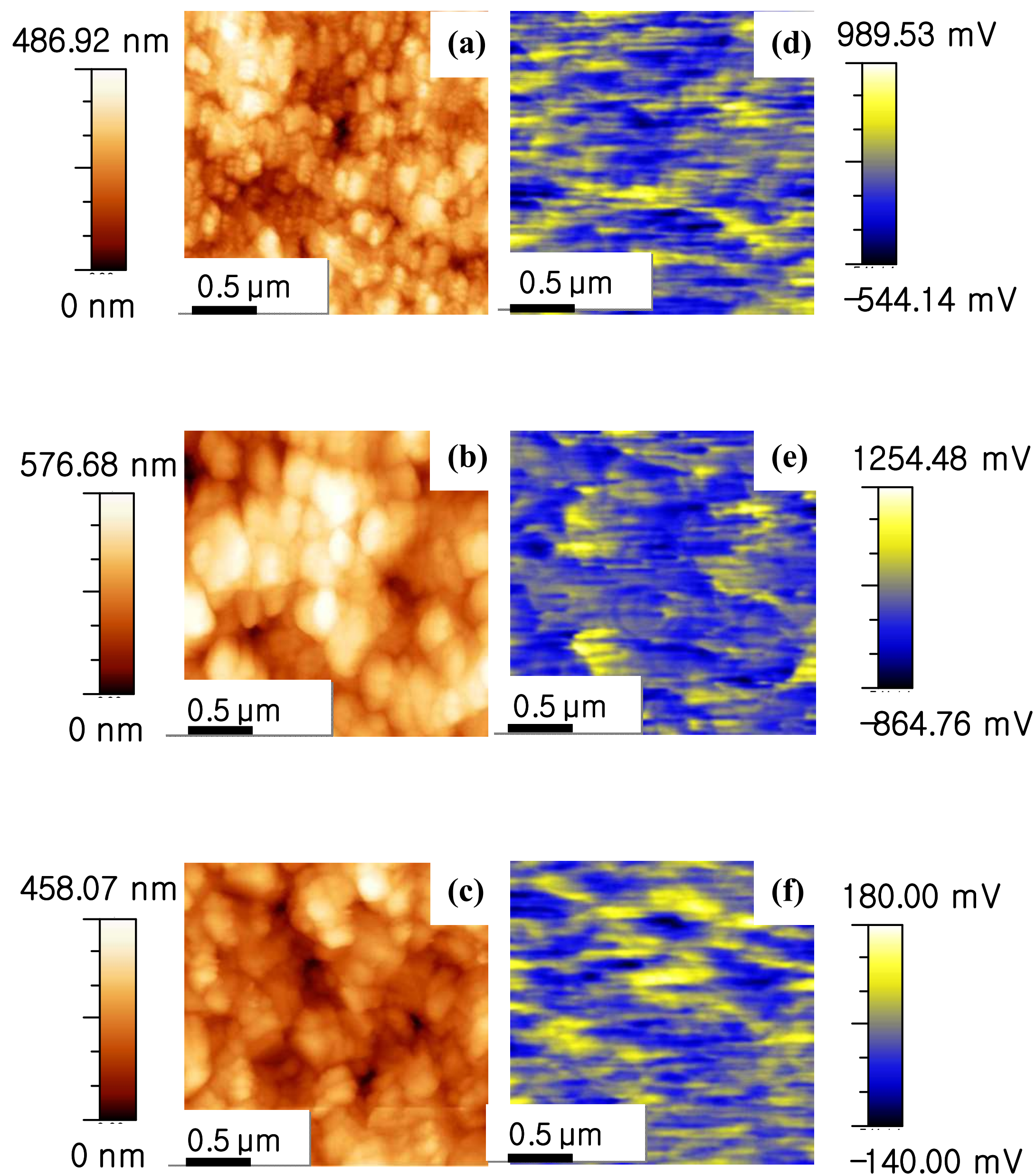

RSC Advances Accepted Manuscript

Figure 6. JungYup Yang *et al.*

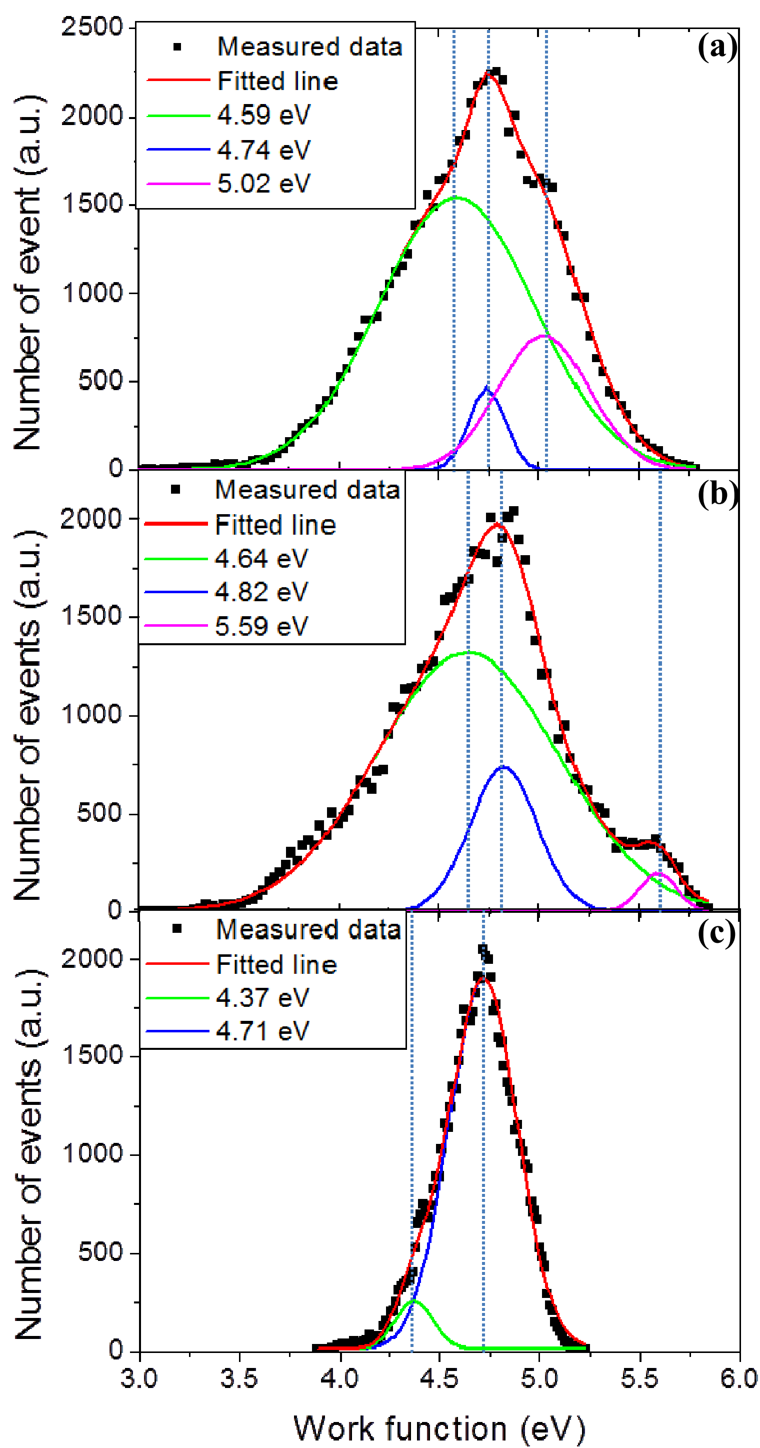

Figure 7. JungYup Yang, *et al.*

RSC Advances Accepted Manuscript

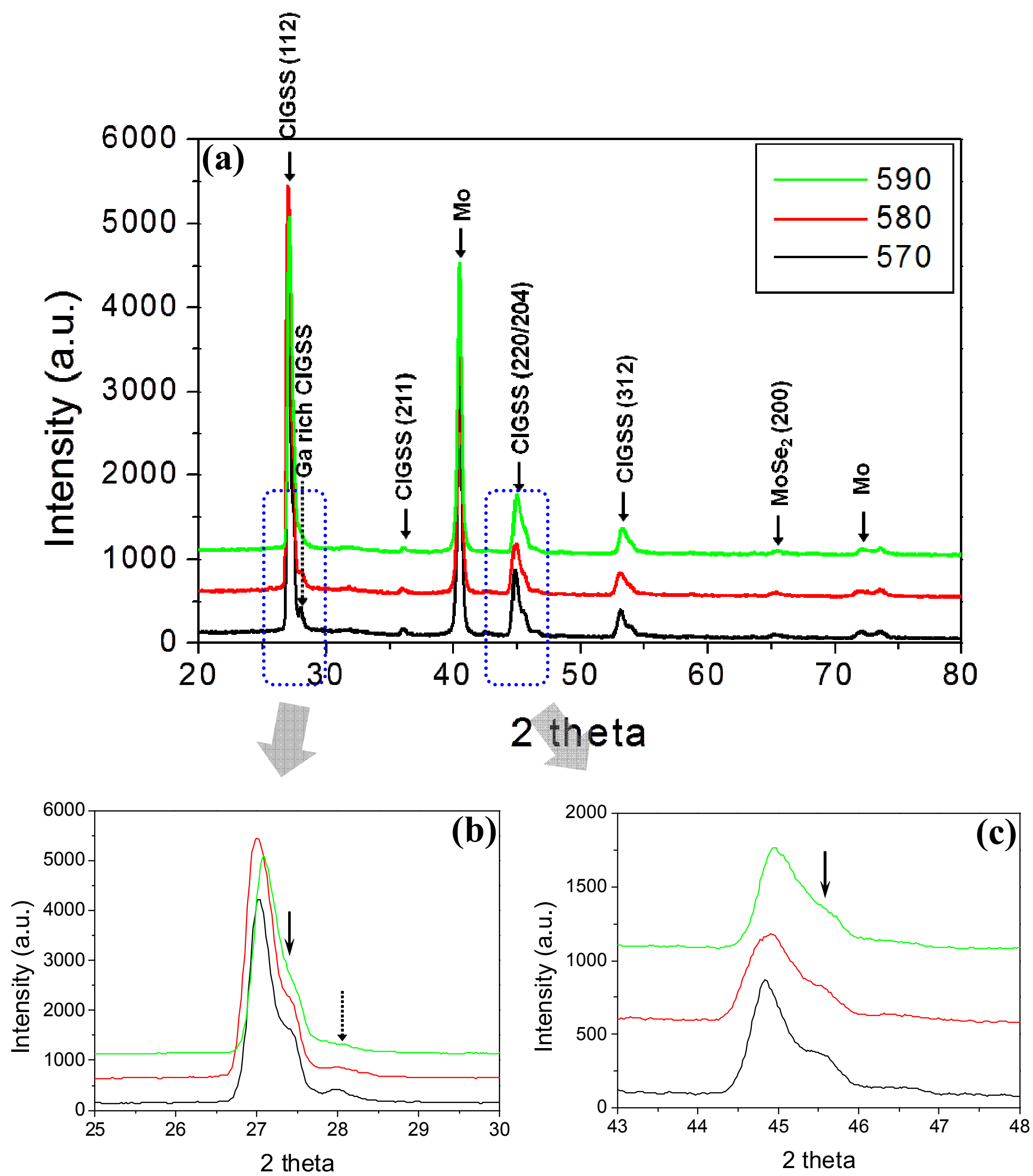

Figure 8. JungYup Yang, *et al.*

RSC Advances Accepted Manuscript

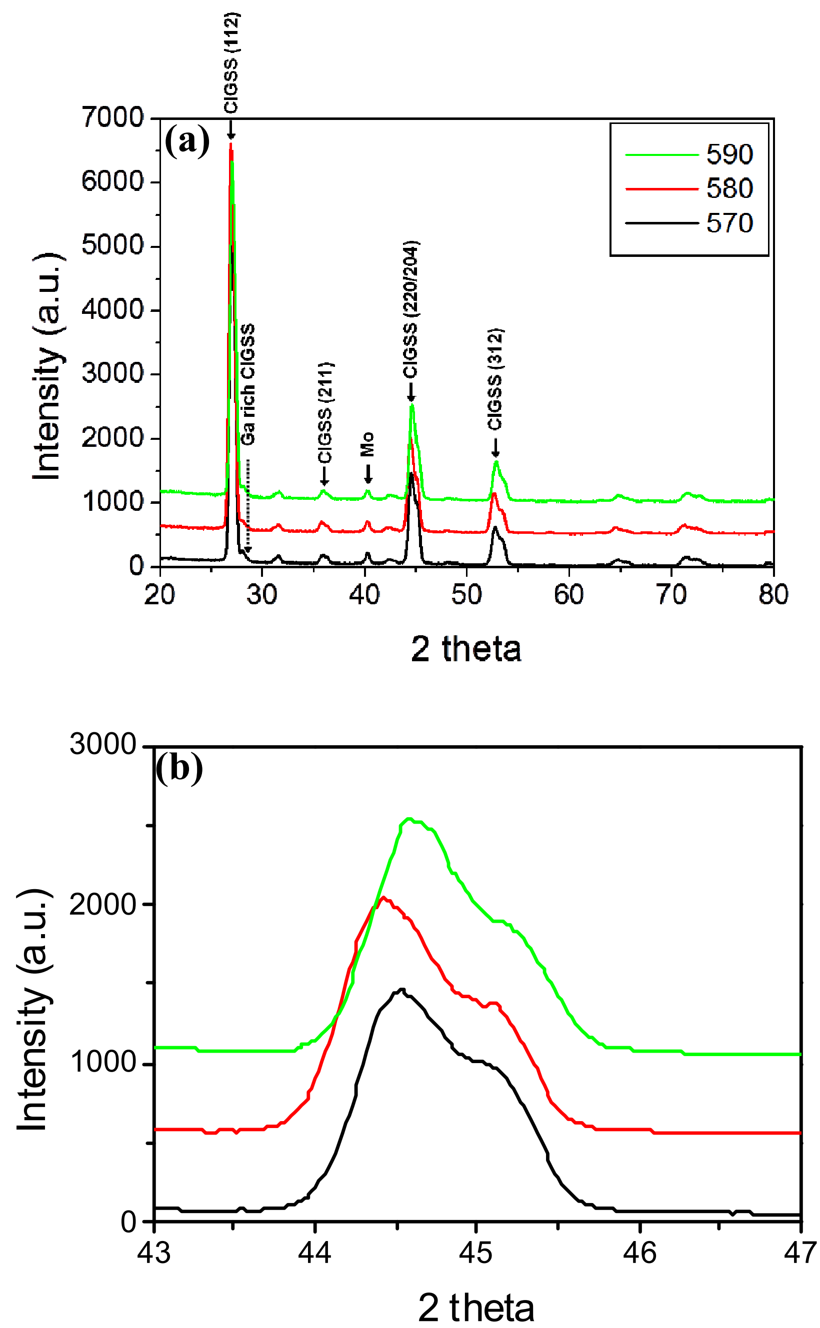

Figure 9. JungYup Yang, *et al.*

RSC Advances Accepted Manuscript

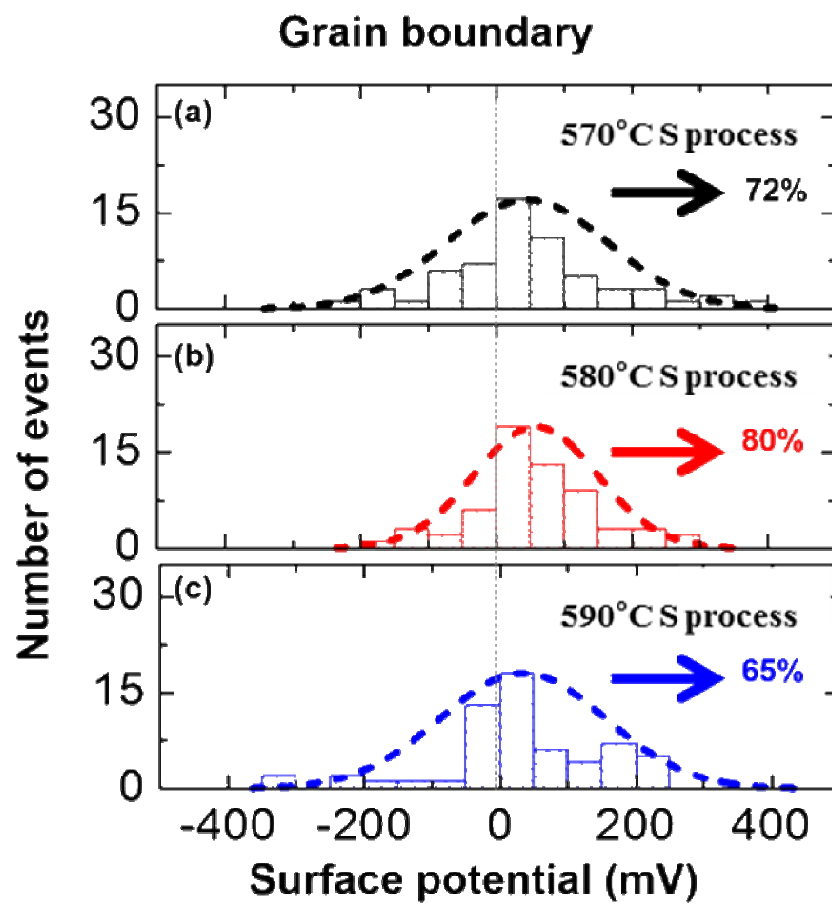

Figure 10. JungYup Yang, *et al.*

RSC Advances Accepted Manuscript

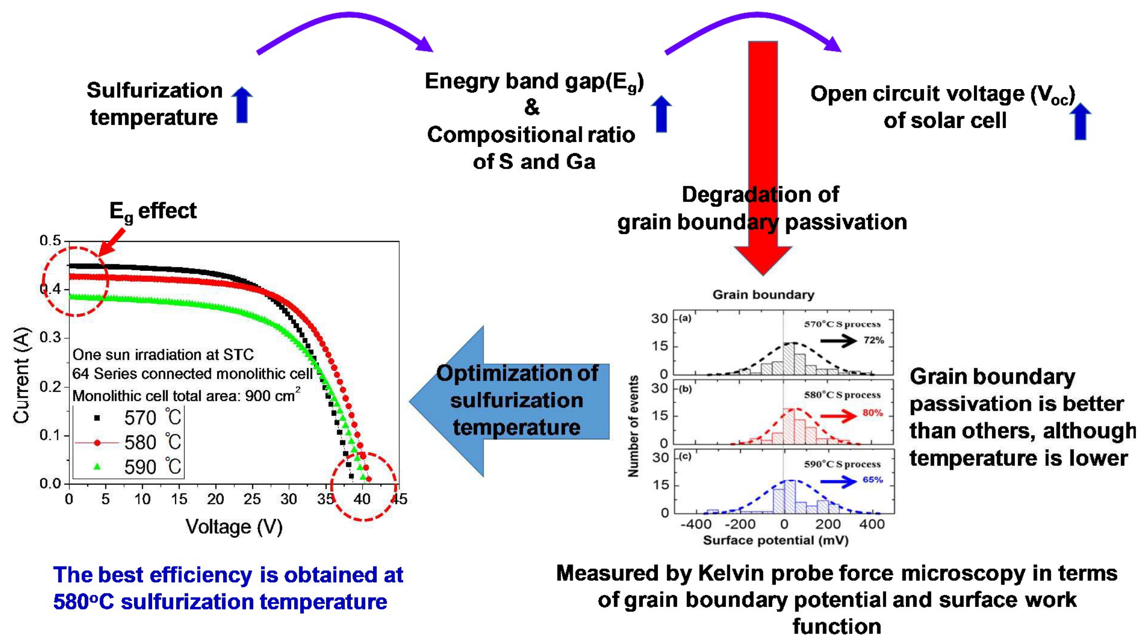

RSC Advances Accepted Manuscript